Results in Physics 55 (2023) 107170

Contents lists available at ScienceDirect

Results in Physics

journal homepage: www.elsevier.com/locate/rinp

Ytterbium-doped fiber laser as a source of coexisting narrow-band thermal light and optical rogue waves: Experimental demonstration

Yuri O. Barmenkov [a,*], Pablo Muniz-Cánovas [a], Vicente Aboites [a], José-Luis Cruz [b], Miguel V. Andrés [b]

[a] Centro de Investigaciones en Óptica, A.C., Loma del Bosque 115, 37150 Leon, Gto., Mexico
[b] Departamento de Física Aplicada, Instituto de Ciencia de Materiales, Universidad de Valencia, 46100 Valencia, Spain

ARTICLE INFO

Keywords:
Ytterbium-doped fiber laser
Photon statistics
Bose-Einstein statistics
Thermal light
Optical rogue waves

ABSTRACT

In this paper, we show that a continuous-wave ytterbium-doped fiber laser implemented in the conventional configuration of a Fabry-Perot cavity with two fiber Bragg gratings as selective reflectors and a moderate output power (tens of watts) generates two groups of photons, each of which is characterized by its own statistics. The statistics of the first group are described by the $M-$fold degenerate Bose-Einstein distribution, where M is the number of independent states of spontaneous emission, which, in turn, depends on the laser linewidth and the radiofrequency band of the recording equipment. This kind of light is classified as narrow-band thermal light. The second group of photons is described by the extreme-value exponential statistics with a probability of encountering extremely large photon events much greater than expected from the Bose-Einstein distribution, which is classified as optical rogue waves. At a low laser power, the first group of photons strongly dominates over the second. As the laser power increases, the fraction of photons of the second group increases monotonically; above a certain threshold, the fraction of this group increases, reaching tens of percent of the total number of laser photons.

Introduction

Ytterbium-doped fiber lasers (YDFLs) are versatile photonics devices that operate in various regimes such as continuous wave (CW), Q-switched, mode-locked including solitons, noise pulses, *etc.* [1–6]. CW double-clad (DC) YDFLs are very efficient light sources with optical-to-optical conversion efficiency as high as 80% [1,7,8] and a wide optical range, from ~ 975 nm to ~ 1180 nm [9–14], with output power scalable up to very high levels, from several kW in single mode [7,8,15] to tens of kW in multi-mode configurations [16–18]. Due to very large power scaling and the perfect energy budget YDFLs found a great number of biomedical [19,20] and industrial applications [21], they can be used as an optical pump for other types of lasers [22–25], for frequency nonlinear conversion [26,27], and so on.

CW-YDFLs implemented using a Fabry-Perot cavity with fiber Bragg gratings (FBGs) as selective reflectors demonstrate high-level intensity (photon) noise that is characterized by the $M-$fold degenerate Bose-Einstein statistics where M is a number of independent states of amplified spontaneous emission (ASE) [28,29]. This kind of intensity noise describes thermal light with a narrow optical band [6,28] which originates from the intensity fluctuations of a narrow-band spontaneous emission (SE) amplified together with the laser wave on each pass along the gain fiber. Recently it was shown that pulses composed of narrow-band thermal light (pulsed ASE source) are twice as efficient in wavelength conversion through second harmonic generation if compared to transform-limited pulses with identical mean photon flux [30].

If the intra-cavity laser power is high enough so that the optical nonlinear effects related to the Kerr nonlinearity play an important role in the laser wave evolution, the laser optical spectrum dramatically broadens [13,31]. This effect leads to a decrease in the effective reflection of the laser output coupler (low reflection FBG) due to a spectral surrounding of its reflection spectrum by the laser wave with a broadened spectrum and, consequently, to decreasing the quality factor of the laser cavity and to increasing the active fiber gain [13]. In turn, the latter may result in arising CW parasite lasing at the wavelength at which ytterbium-doped fiber (YDF) gain has a maximum (1.06–1.09 μm) when YDFL operates in the long wavelength range (1.12–1.20 μm), which decreases the laser efficiency and also can ignite SBS pulsing

* Corresponding author.
E-mail address: yuri@cio.mx (Y.O. Barmenkov).

https://doi.org/10.1016/j.rinp.2023.107170
Received 24 July 2023; Received in revised form 2 November 2023; Accepted 5 November 2023
Available online 8 November 2023

potentially dangerous for the active fiber [32].

In this paper, we discuss the photon statistics of a CW-DC-YDFL with random polarization, moderate output power (30 W), and broadened optical spectrum in detail. All experimental histograms of the laser power were analyzed in the broad range of the photon noise magnitudes, of approximately 100 dB of difference between the maximum and minimum values of the photon noise power, considering the noise histogram of the registering equipment. To make the photon statistics clearer, we used polarized laser light for the experimental study.

We show that the laser signal consists of two groups of photons: the first group is characterized by the Bose-Einstein statistics with a degeneracy factor M equal to the number of independent states of amplified spontaneous emission in the laser signal, which is defined by the ratio B_{opt}/B_{el} (B_{opt} is the laser linewidth and B_{el} is electrical bandwidth of the receiving equipment, both in Hz). The second group of photons is described by the exponential distribution, which is observed usually when $B_{opt} \ll B_{el}$. (Generally, an exponential distribution is a case of the Bose-Einstein statistics when $M = 1$.) We show that the reciprocal exponential decay constant of this distribution that should be equal to the average number of photons of the second group detected by PD during the integration time $\Delta t = 1/B_{el}$ (the value that relates to the mean laser power), is much larger than expected, so the absolute slope of the photon count distribution is much smaller and, therefore, a probability of encountering extremely large photon events is very high. These strong photon events with unexpectedly high probability can be classified as optical rogue waves.

We also show that as the laser power grows, the part of laser photons characterized by the exponential statistics increases strongly, despite the fact that the width of the laser spectrum and, as a consequence, the $M-$factor increase. At high laser power, the number of photons related to optical rogue waves reaches tens of percent in the total number of photons generated by the laser.

Note that the first observation of the rogue waves in optics was related to the experiments with supercontinuum generation in photonic crystal fibers using YDFL as a pump source was reported in Ref. [33] in which the correspondent link between rogue waves in optics and the ocean was established for the first time. It is worth mentioning the important overviews of the optical rogue waves were presented in Refs. [34,35].

We believe that the presented work allows one to clearly understand the physics behind CW operation of YDFL important for applications.

Laser setup and basic characteristics

The YDFL studied was implemented in a Fabry-Pérot cavity configuration commonly used in high-power fiber lasers (FLs). The experimental setup is shown in Fig. 1(a). A commercially available DC-YDF (Coherent, SM-YDF-5/130-VIII) was used as a gain medium. The YDF was bent on an aluminum cylinder with 18-cm outer diameter and length $L_{YDF} = 12$ m, which provides 20-dB DC absorption at the pump wavelength (975 nm). Two 30-W laser diodes (LD1 and LD2) with multimode outputs were used for pumping the YDF through a commercial $(2 + 1) \times 1$ multimode pump combiner.

Two home-made fiber Bragg gratings (FBGs) were used as the laser cavity mirrors: the first one (FBG1) with a reflection of 100%, as the rear mirror, while the second one (FBG2) with a reflection of $R_{out} = 21\%$, as the output mirror. The laser cavity length found as a fiber length between FBGs was $L_c = 13.5$ m. FBGs' reflection bandwidths measured as FWHM measured using an optical spectrum analyzer (OSA) (Yokogawa AQ6370D) with 34 pm-resolution at the laser wavelength were 220 pm and 44 pm, respectively. Both FBGs were written in a single-mode fiber with the Bragg wavelength at $\lambda_s = 1061$ nm (the laser wavelength).

A cladding mode stripper (CMS) was used to damp the residual pump at the FBG2 input. To decrease the parasite reflection from both laser sides we used 7°-fiber cuts. The in-line polarizer with PANDA fiber tails placed at the photodetector (PD) input was used (not shown), which allowed one to decrease the number M of independent states of spontaneous emission by a factor of two.

The laser output power characteristics are shown in Fig. 1(b), from which the laser optical-to-optical conversion efficiency was estimated as 70%; the laser threshold pump power was 1.5 W. The broad-band laser spectra measured at different pump powers with a resolution of 0.5 nm are shown in Fig. 1(c). The spectra do not demonstrate any inhomogeneities or peaks related to Brillouin or Raman scattering. Fig. 2 shows a typical oscilloscope trace of the laser signal registered by a 25-GHz photodetector (*Newport*, model 1414) connected with a 16-GHz real-time oscilloscope (*Tektronix*, DPO71604C); the cumulative RF band of this set of devices is 15.5 GHz. From this figure, one can see that YDFL operates in a quasi-CW regime characterized by random noise pulsing with random amplitudes, widths, and intervals of sequence (see also Refs. [6]).

Experimental results and discussion

Narrow-band optical spectra and M−factor

The YDFL narrow-band optical spectra were measured in the whole range of laser power using OSA with a resolution of 34 pm, see Fig. 3(a). From this figure one can see that the laser spectra dramatically broaden with increasing laser power, the effect observed in powerful CW-YDFLs.

All the spectra were fit using Gaussian law for further deconvolution of the laser spectra. This procedure considers the fact that the OSA spectral response on the extremely narrow-line laser signal (DFB semiconductor laser with 130 kHz-optical linewidth) is almost Gaussian. In

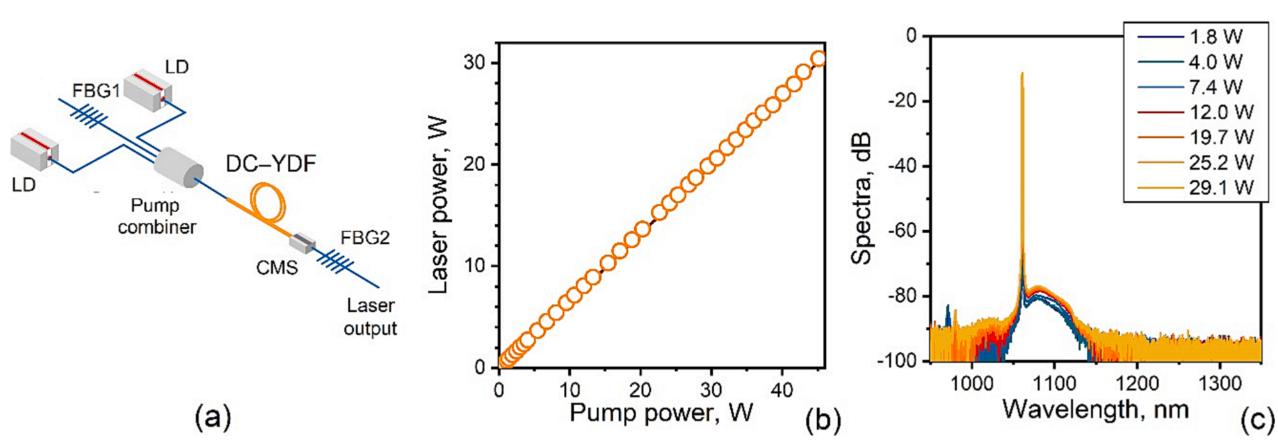

Fig. 1. (a) YDFL setup. (b) YDFL power *vs*. pump power. (c) YDFL spectra *vs*. laser power. The values of laser power are shown in the inset.

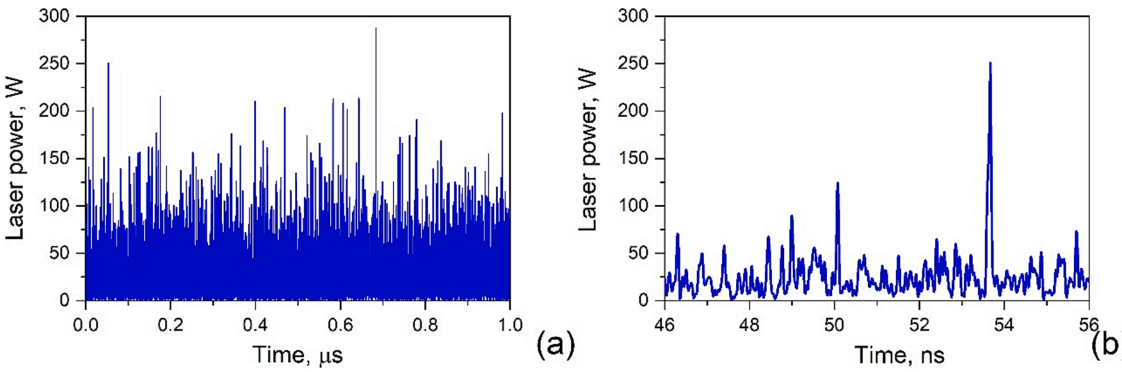

Fig. 2. Typical laser trace in the large (a) and the short (b) time intervals. The laser mean power is 23.2 W.

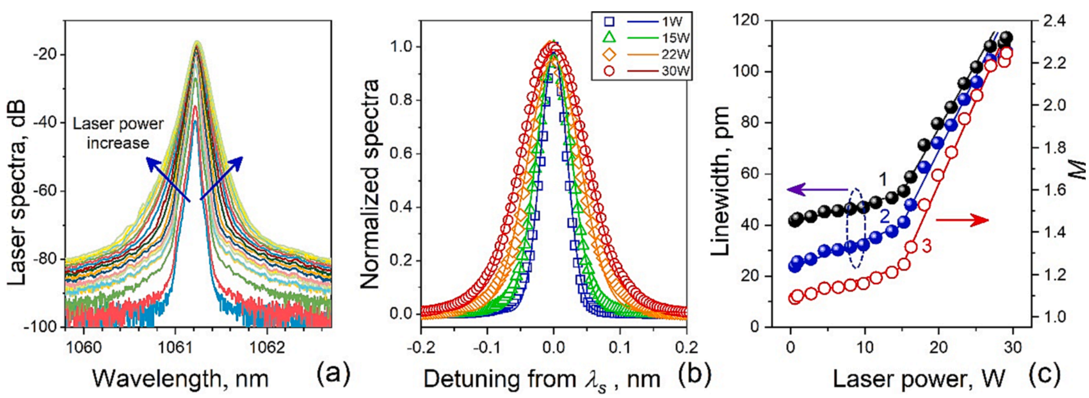

Fig. 3. (a) Laser spectra measured in the whole range of YDFL power. The minimum power is 0.53 W (the bottom blue curve) and the maximum power is 30 W (the upper gray curve). The power at which the spectra were measured corresponds to that of the experimental points shown in Fig. 2(c). (b) Normalized laser spectra (linear scale). The symbols are experimental points and the solid curves are fits by the Gaussian function. The powers at which the spectra were measured are shown in the inset. (c) The measured (black circles, curve 1) and deconvoluted (blue circles, curve 2) values of the YDF linewidth *vs*. laser power, the left scale. $M-$values *vs*. laser power (the red circles, curve 3), the right scale (curve 3). (For interpretation of the references to colour in this figure legend, the reader is referred to the web version of this article.)

the whole range of the laser power the spectra are fit by the Gaussian function with the residual sum R^2 better than 0.99, see Fig. 3(b) in which the laser spectra measured at four power values are shown. Note that the Gaussian shape of the laser line is important for the calculation of the $M-$factor using the known laser spectrum width (B_{opt}) since the analytical solution used for the simulation is derived for the Gaussian spectrum (see chapter 6 in ref. [28]):

$$M = s\frac{\pi\left(B_{opt}/B_{el}\right)^2}{\pi\left(B_{opt}/B_{el}\right)\mathrm{erf}\left[\sqrt{\pi}\left(B_{opt}/B_{el}\right)\right] - \left[1-\exp\left(-\pi\left(B_{opt}/B_{el}\right)^2\right)\right]} \quad (1)$$

where s is the number of polarization states (one or two) and erf is a standard error integral.

The measured and deconvoluted laser linewidths are presented in Fig. 3(c) together with the $M-$values calculated using Eq. (1). It is seen that the deconvoluted (real) spectrum width monotonously increases as the laser power grows. At laser power below the specific value $P_0 \approx 15$ W the slope of this dependence is about 1 pm/W, while at laser power above P_0 the slope increases by approximately 6 times, to about 6 pm/W. The $M-$factor shows a similar behavior: it increases initially with the laser power growth with the slope of 0.0085/W, but above P_0 the slope increases by an order, to 0.08/W.

The value of the laser power $P_0 \approx 15$ W at which the slopes are dramatically increased is related to the self-phase modulation of the laser wave propagating along the YDFL cavity. Considering the YDF gain is a constant along the cavity [36] (approximation frequently considered for CW-DC-YDFL simulation) and that $L_{YDF} \approx L_c$, and accounting for the effective reflection of the output mirror of the laser cavity (FBG2) R_{eff} as the third part of R_{out} [6], the YDF gain is found as $g = \ln(R_{eff}{}^{-1})/(2L_c) = 0.1\ \mathrm{m}^{-1}$. Thus, when $P_{out} = P_0$, the averaged power P_{avg} of the laser wave reflected by FBG2 and propagated along the amplifying fiber to FBG1 and then back to FBG2 is given by

$$P_{avg} = \frac{R_{eff}}{1-R_{eff}}P_0\frac{1}{2L_c}\int_0^{2L_c} e^{gz}dz = 5.5\mathrm{W} \quad (2)$$

where R_{eff} /(1-R_{eff}) is the fraction of laser power reflected by FBG2 back to the laser cavity.

Considering the known P_{avg} and the fiber parameters as the nonlinear refractive index $n_2 = 4.3 \times 10^{-20}$ m^2/W at 1060 nm [37] and the effective area of the laser beam in the fiber $A = \pi(\mathrm{MFD}/2) = 34$ µm^2 (MFD is the mode-field diameter at 1060 nm), one can easily obtain that the nonlinear fiber length L_{NL} is 25 m $\approx 2L_c$, at which the nonlinear phase $\varphi_{NL} = \pi$ [38]. Thus, when the laser power P_{out} increases to 15 W the nonlinear phase reaches the π-value, above which the laser spectrum and the $M-$factor dramatically increase with further laser power growth.

Note that the $M-$factor values obtained will be used for detailed simulation of the laser photon statistics, as shown below.

Accounting for photodetector noise in the fitting of the photon count histograms: Theory

Since the experimental histograms of the laser photon count distributions (or probability density functions, PDFs) demonstrate very large tails, with events that randomly reach power by up to two orders higher or even more than the mean (CW) laser power P_{mean}, we had to attenuate the laser signal so that PD used in the experiments is far from saturation. In this case, the PD noise affects photon statistics because each experimental point of the photon PDF is a convolution of the real photon statistics and the PD noise statistics:

$$P_{exp}(n) = A\sum_{-K}^{K} P(n-k)\text{Gauss}(k) \tag{3}$$

where $P_{exp}(n)$ is the normalized experimental PDF for n photons registered by the PD (photoelectrons) during the integration time $\Delta t = 1/B_{el}$, k is a number of electrons generated randomly in PD during Δt (proportional to PD instantaneous noise voltage), $P(n)$ is the PDF described by the $M-$fold degenerate Bose-Einstein distribution (MBED) (see chapter 9 in ref. [28]):

$$P(n) = \frac{(n+M-1)!}{n!(M-1)!}\frac{(\overline{n})^n}{(1+\overline{n})^{n+M}} \tag{4}$$

In Eq. (3) above, Gauss is the Gaussian function, K characterizes the range in which the noise PD dark voltage fluctuates, and A is the proportionality coefficient used for the PDF normalization. The photon number n changes from zero to tens of the mean photon number $\overline{n}$. Since the normalized histograms practically do not vary for $\overline{n} \geq 200$ [39], we used $\overline{n} = 200$ in calculations. Note that in the absence of the PD noise, a photon number n registered by PD during Δt is proportional to the instantaneous laser power.

The PD dark current noise histogram is shown in Fig. 4(a), which is fit by the Gaussian function with $R^2 = 0.99998$. A slight shift of the histogram to positive values (0.176 mV) will be used for correcting the PDFs of the laser photons.

Two examples of the photon distribution modeled with allowance for the PD noise histogram for $M = 1$ and $M = 2$ are shown in Fig. 4(b) and 4 (c), respectively. The horizontal axes are shown in the photon number normalized to the mean photon number; the bottom insets show values of the standard deviation w at which the distributions were simulated. From these figures, it is possible to conclude that with increasing w the normalized PDF of phonon count broadens and its peak shifts to the right direction, both effects may be associated with a change in the $M-$factor if the PD noise is not considered. Therefore, PD noise must be considered for a correct $M-$factor calculation.

Fitting of the experimental photon count histograms

Fig. 4 shows three examples of fitting the experimental histograms of photon distribution when PD noise is considered. The histograms are presented as PDFs of the PD voltage (proportional to photon count) normalized to its maximum *versus* the instantaneous laser power (proportional to the photon number n) normalized to the mean laser power. The histograms simulated by MBED without and with consideration for the PD noise distribution are shown for comparison.

The first observation is that the photon statistics is more complex than the one described by MBED only: at low instantaneous powers, from zero to a few mean laser power, it is fitted with high precision by BMED accounting for PD noise and using $M-$factor found from the laser linewidth (Fig. 3(c)). At higher instantaneous power the absolute slope of the experimental histogram dramatically decreases; the fit in this case can be realized by a sum of MBED and a number of the exponential functions with different decay constants. Note that MBED with $M = 1$ is the exponential distribution with a decay constant equal to the mean number of photons $\overline{n}$ (proportional to the mean laser power) considered in the experiment.

When the mean laser power is low (see Fig. 5(a)) multiple exponential functions are used for fit (the fit shown in the graph was performed by MBED and five exponentials). The maximum of instantaneous laser power observed at the normalized PDF level of 5×10^{-10} (the registration equipment limit) is approximately two orders higher than the mean laser power. The negative PDF values are observed due to the negative fraction of the PD noise (see Fig. 4(a)).

At higher mean power ($P_{mean} \geq 4$ W) the experimental PDF is fit by a sum of MBED and two exponentials, one of them fits the histogram tail and another one the transition area between MBED and the tail, see Fig. 5(b) in which the experimental and simulated histograms are shown for $P_{mean} = 5.4$ W. Note that only the exponential that fits the experimental histogram tail is of our interest since it describes the high power photon events, so the other one is omitted. The reciprocal decay constant of the exponential that fits the PDF tail is 34 W which is 6.3 times higher than the mean power of the photons described by MBED (see curves 2 and 3 in Fig. 3(b)) while their averaged power (photon number registered during Δt) is negligible as compared to P_{mean}.

With further P_{mean} increase, the transient area between the parts of the photon count histogram described by MBED and the exponential histogram tail gets shorter, and at $P_{mean} > 10$ W this area disappears. In such circumstances the photon count histograms are fit by MBED and a single exponential function, see Fig. 5(c) in which the histograms are plotted for $P_{mean} = 16.2$ W. It is seen that the exponential function fits

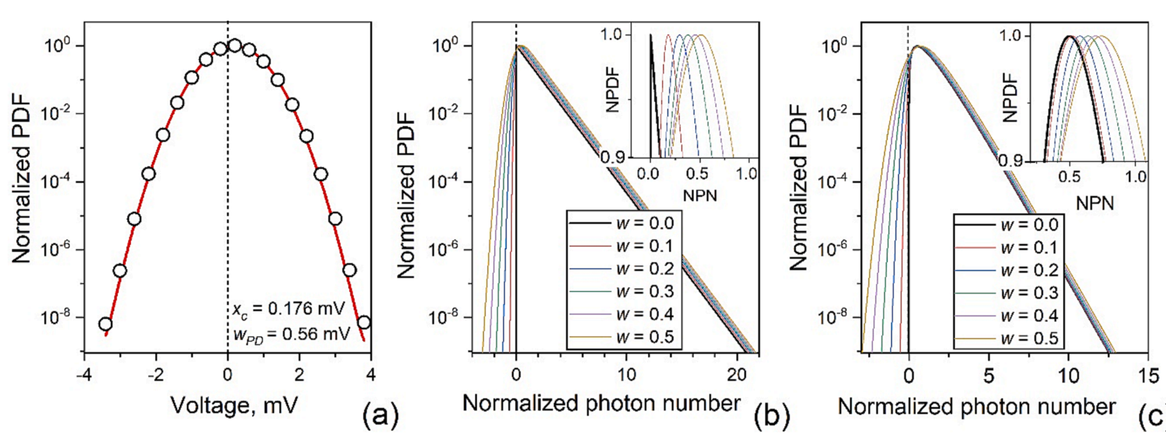

Fig 4. (a) Normalized histogram of the photodetector noise: the circles are the experimental points and the solid curve is the Gaussian fit. The standard deviation is $w_{PD} = 0.56$ mV and the peak position $x_c = 0.176$ mV. Convolution of the photon count distribution characterized by (b) $M = 1$ and (c) $M = 2$ and the photodetector noise histogram for different values of the standard deviation w normalized to the PD voltage at P_{mean} (the bottom insets) *vs.* the photon number n normalized to the mean photon number $\overline{n}$. Insets in the top right corner show the zoomed area near the histograms' peaks in linear scale. NPN is the normalized photon number and NPDF is the normalized PDF.

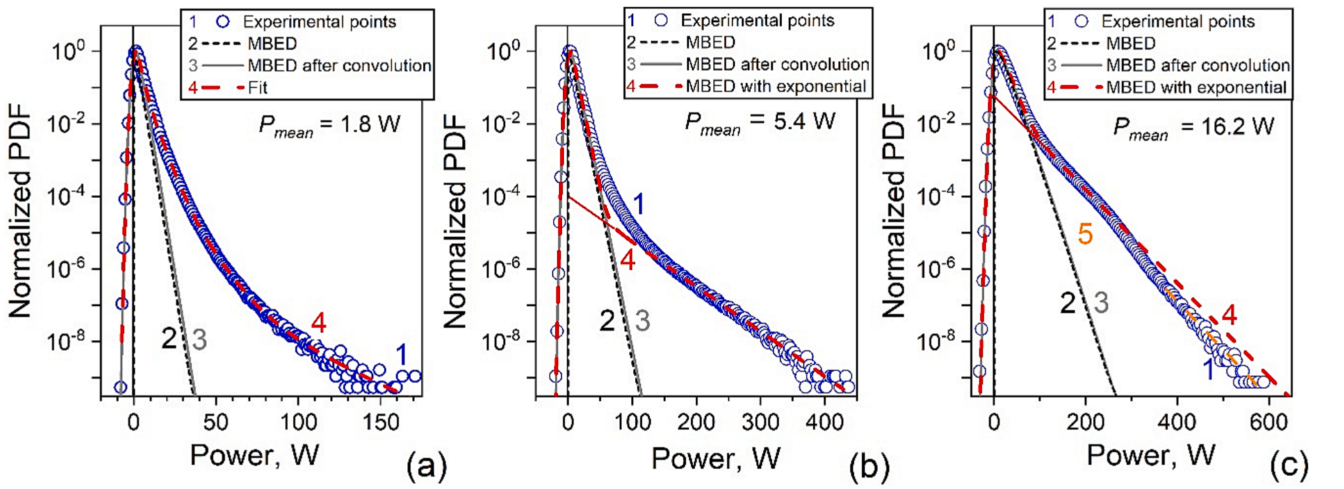

Fig 5. Normalized PDF of photon count found at (a) $P_{mean} = 1.8$ W, (b) $P_{mean} = 5.4$ W and (c) $P_{mean} = 16.2$ W. Curves marked by 1 are the experimental PDFs, by 2 are MBED, by 3 are MBED after convolution by the PD noise histogram, and by 4 are fits of the experimental points by a sum of the convoluted MBED and the exponential decay functions (plot (a)) or a lone exponential function (plots (b) and (c)). The red solid lines shown in (b) and (c) are continuations of the exponential decays to zero power. (For interpretation of the references to colour in this figure legend, the reader is referred to the web version of this article.)

the histogram tail in the range of the instantaneous laser power from 150 W to 320 W, with the decay constant equal to 37 W, the value slightly higher than in the case of $P_{mean} = 5.4$ W. At the instantaneous laser power above 300 W the histogram tail drops by ~ 5 times, maintaining approximately the same exponential decay constant in the instantaneous power above 400 W (see the orange dash line).

Resume of the experimental results

Fig. 6(a) shows a set of selected experimental histograms of photon counts and corresponding approximations by the sum of MBED and exponential functions obtained over the entire laser power range (1.8 W to 30 W). At the CW laser power greater than or equal to 4 W, the histograms' tails are fit by a single exponential function with the reciprocal decay constant that slightly increases (see the green area A), from 34 to 44 W with the mean laser power growth.

In the range of the instantaneous power from ~ 300 W to ~ 400 W the exponential fitting drops to some new level and then continues decreasing with approximately the same decay constant (see the blue area B). Above 600 W of the instantaneous laser power the fitting drops one more time to some level. Studying this process below the 10^{-8} level of the normalized PDF is difficult due to excessive noise. Note that with increasing of the mean laser power the drops' magnitudes decrease, from 5 times at 16.2 W of the mean laser power to 1.5 times at 29.1 W. We assume that the drops in the exponential distribution tails arise from the laser spectrum broadening: the rear fiber Bragg grating (FBG1) does not reflect the spectral components far from the Bragg wavelength; on the propagation of the laser wave to FBG2 the broadening process recovers but with smaller magnitude.

The exponential fitting function drops by about two orders of magnitude within the area A, so the number of photons described by the exponential statistics counted in the range of instantaneous power from zero to ~ 320 W is much greater than that counted in the range of powers above this value. Thus, one can estimate the contributions of the photons characterized by MBED and by the exponential distribution in the total photon number.

For this purpose, we integrated separately the areas under the curves corresponding to the MBED and the exponential distribution (see Fig. 5 (b) and (c)), and then divided each of them by the sum of these areas, see Fig. 6(b) that shows the result of this procedure. It is seen that at a laser

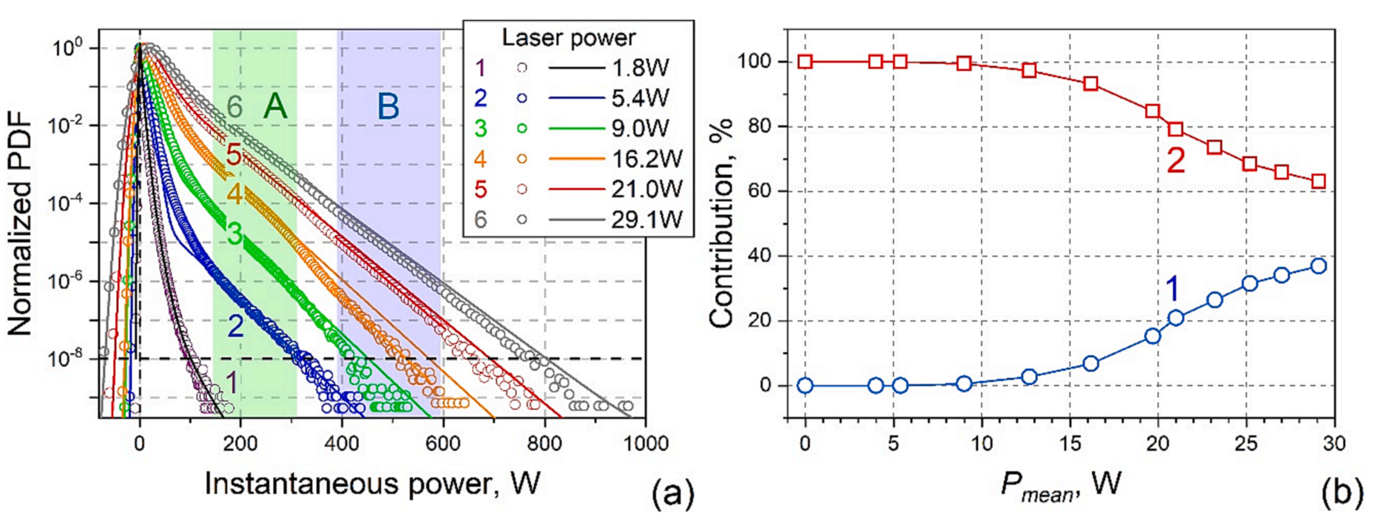

Fig 6. (a) Experimental histograms of photon counts for selected laser powers (see inset). Circles are experimental points and solid curves are fits. (b) Contribution of the photons with statistics described by MBED (red square symbols and line 2) and by exponential distribution (blue circles and line 1) *vs.* the mean laser power. (For interpretation of the references to colour in this figure legend, the reader is referred to the web version of this article.)

power of less than 10 W, the contribution of the photons with exponential statistics (curve 1) is almost negligible. A noticeable contribution, about 5%, is observed at a laser power of 15 W. As the laser power increases to 30 W, the contribution of photons with exponential statistics increases to about 40%. At the same time, the contribution of the photons with statistics described by MBED (curve 2) decreases so the sum of both contributions is 100%. We believe that at further increasing the laser power the contribution of photons with extreme-value exponential statistics can reach 100%.

Thus, we may conclude that YDFL at moderate laser power generates two groups of photons that differ in statistics: the first group is described by the $M-$fold degenerate Bose-Einstein distribution with $M-$factor found from the laser optical spectra and the second group by the exponential distribution. The important observation is that the photon histogram of the second group of photons demonstrates the absolute slope much smaller than it should be observed in accordance with the mean laser power since the exponential decay constant corresponds to a much higher power. For instance, if the real mean power is 16.2 W the contribution of the second group of photons is 6.8% (see Fig. 6(b)). The mean power that corresponds to this group of photons is 1.1 W, not 37 W as it follows from the exponential decay constant, so the difference is 34 times. In the case of the laser power of 29.1 W this difference is smaller, 4.2 times, which is explained by a strong increase in the contribution of this group of photons in the laser signal.

Note that a group of photons characterized by the exponential count distribution can be classified as random optical rogue waves since they are described by extreme-value statistics. Note also that the main characteristic of rogue waves in both fluid mechanics and optics is the height of the waves which is dramatically larger than that of conventional waves (in our case narrow-band thermal light waves). Each point of the histograms of the instantaneous laser power (Fig. 6 (a)) shows the probability of detection of a certain level of instantaneous power of the random noise pulses, which includes the peak power of the pulses. Therefore, it can be concluded that the magnitudes of the optical rogue waves detected at the laser output reach values of about 1 kW when the average laser power is 30 W. The pulses with higher magnitudes occur with a lower probability.

Conclusions

In this paper, we have discussed the peculiarities of the photon statistics of a continuous-wave double-clad ytterbium-doped fiber laser. We demonstrated that the laser operates in the regime of random noise pulses that is composed of two coexisting groups of laser photons that differ in statistics: the photon counts of the first (typical) group are described by the $M-$fold degenerate Bose-Einstein distribution with the $M-$value dependent on the ratio of B_{opt} to B_{el} (B_{opt} is the laser linewidth and B_{el} is the photodetector electrical bandwidth). This type of light, similar to the narrow-band spontaneous emission, is classified as a narrow-band thermal light. The second group of the laser photons is characterized by the extreme-value exponential statistics at which the probability of encountering high-power photon events is much larger than expected from the Bose-Einstein statistics including the case of $M = 1$, which corresponds to the exponential distribution with the decay constant equal to the reciprocal mean laser power. This group of photons can be classified as random optical rogue waves.

At low laser power, the first group of photons related to the narrow-band thermal light is strongly dominant. When laser power is above the value at which the nonlinear length is equal to a double-pass of the laser wave along the laser cavity, the second group of photons related to rogue waves increases sharply, reaching about 40% of the total photon number at the maximum laser power (30 W). We believe that this group of photons will be dominant with further increasing of laser power, and the laser will turn to the mode of optical rogue waves' operation.

The results of the presented study are important for understanding the physics behind CW operation of the ytterbium-doped fiber lasers since the rogue-wave laser operation may find some specific applications in the future.

Funding

This work was supported in part by the CONAHCyT, Mexico (Project No. CF-2023-I-2431), the Ministerio de Ciencia e Innovación/Agencia Estatal de Investigación, Spain (MCIN/AEI/ https://doi.org/10.13039/501100011033), co-funded by the European Union "ERDF A way of making Europe", under grant PDI2019-104276RB-I00, and the Generalitat Valenciana, Spain (CIPROM/2022/30).

CRediT authorship contribution statement

Yuri O. Barmenkov: Formal analysis, Funding acquisition, Investigation, Validation, Writing – original draft. **Pablo Muniz-Cánovas:** Data curation, Investigation, Writing – review & editing. **Vicente Aboites:** Formal analysis, Investigation. **José-Luis Cruz:** Formal analysis, Investigation. **Miguel V. Andrés:** Funding acquisition, Supervision, Writing – review & editing.

Declaration of Competing Interest

The authors declare that they have no known competing financial interests or personal relationships that could have appeared to influence the work reported in this paper.

Data availability

Data will be made available on request.

References

[1] Richardson DJ, Nilsson J, Clarkson WA. High power fiber lasers: current status and future perspectives [Invited]. J Opt Soc Am B 2010;27(11):B63–92. https://doi.org/10.1364/JOSAB.27.000B63.
[2] Liu T, Yan M, Guo Z, Zeng H. Mechanisms of dual-wavelength dissipative soliton mode-locking in net-normal dispersion fiber lasers. Res Phys 2022;36:105464. https://doi.org/10.1016/j.rinp.2022.105464.
[3] Huang Y, Zhang L, Chen NK, Xie Y, Zhang X, Tian X, et al. Generation of dissipative solitons and self-similar pulses by a mode-locked fiber laser using a bandwidth tunable Mach-Zehnder interferometer filter. Res Phys 2022;42:106035. https://doi.org/10.1016/j.rinp.2022.106035.
[4] Barmenkov YO, Kir'yanov AV, Andrés MV. Experimental Study of the Nonlinear Dynamics of an Actively Q-Switched Ytterbium-Doped Fiber Laser. IEEE Quant Electron 2012;48(11):1484–93. https://doi.org/10.1109/JQE.2012.2220530.
[5] Ustimchik VE, Stoliarov DA, Korobko DA, Chamorovskii YK, Filippov VN. Passively Q-switched 0.24 mJ ring laser based on anisotropic tapered fiber. Res Phys 2021;20:103640. https://doi.org/10.1016/j.rinp.2020.103640.
[6] Muniz-Cánovas P, Barmenkov YO, Kir'yanov AV, Cruz JL, Andrés MV. Ytterbium-doped fiber laser as pulsed source of narrowband amplified spontaneous emission. Sci Rep 2019;9:13073. https://doi.org/10.1038/s41598-019-49695-9.
[7] Jeong Y, Sahu JK, Payne DN, Nilsson J. Ytterbium-doped large-core fiber laser with 1.36 kW continuous-wave output power. Opt Express 2004;12(25):6088–92. https://doi.org/10.1364/OPEX.12.006088.
[8] Zheng J, Zhao W, Zhao B, Hou C, Li Z, Li G, et al. 4.62 kW excellent beam quality laser output with a low-loss Yb/Ce co-doped fiber fabricated by chelate gas phase deposition technique. Opt Mater Express 2017;7(4):1259–66. https://doi.org/10.1364/OME.7.001259.
[9] Fu S, Li L, Zhu X, Norwood RA, Peyghambarian N. 10-W Level Picosecond Yb3+-Doped All-Fiber Laser Source at 976 nm. J Lightw Technol 2022;40(13):4415–9. https://doi.org/10.1109/JLT.2022.3163206.
[10] Wu H, Li R, Xiao H, Leng J, Zhou P. Comprehensive investigations on the tandem pumping scheme employing the pump fiber laser operating at an extremely short wavelength. Opt Expr 2021;29(22):34880–91. https://doi.org/10.1364/OE.434218.
[11] Meng X, Ye Y, Yang B, Xi X, Wang P, Shi C, et al. Demonstration of 3 kW-Level Nearly Single Mode Monolithic Fiber Amplifier Emitting at 1050 nm Employing Tapered Yb-Doped Fiber. IEEE Photon J 2023;15(4):1501507. https://doi.org/10.1109/JPHOT.2023.3277201.
[12] Jacquemet M, Mugnier A, Le Corre G, Goyat G, Pureur D. CW PM Multiwatts Yb-Doped Fiber Laser Directly Emitting at Long Wavelength. IEEE J Select Topics Quant Electron 2009;15(1):120–8. https://doi.org/10.1109/JSTQE.2008.2010832.
[13] Barmenkov YO, Muniz-Cánovas P, Kir'yanov AV, Aboites V, Cruz JL, Andrés MV. Power-dependent effective reflection of fiber Bragg grating as output coupler of

Ytterbium-doped fiber laser. Res Phys 2022;42:105980. https://doi.org/10.1016/j.rinp.2022.105980.
[14] Zhou P, Li R, Xiao H, Huang L, Zhang H, Leng J, et al. Exploring high power, extreme wavelength operating potential of rare-earth-doped silica fiber. Proc SPIE 2017;10339:103391C. https://doi.org/10.1117/12.2269614.
[15] Lin W, Desjardins-Carrière M, Iezzi VL, Vincelette A, Bussières-Hersir MH, Rochette M. Simple design of Yb-doped fiber laser with an output power of 2 kW. Opt Las Technol 2022;156:108448. https://doi.org/10.1016/j.optlastec.2022.108448.
[16] Zervas MN, Codemard CA. High power fiber lasers: A review, IEEE. J Sel Topics Quant Electron 2014;20(5):0904123. https://doi.org/10.1109/JSTQE.2014.2321279.
[17] Ferin A, Gapontsev V, Fomin V, Abramov A, Abramov M, Mochalov D. 31.5 kW CW fiber laser with 100 μm delivery, presented at 15th Int Conf Laser Opt., St. Petersburg, Russia 2012; paper TuSY1-1.4. https://doi.org/10.1364/ASSL.2013.ATh4A.2.
[18] Shcherbakov EA, Fomin VV, Abramov AA, Ferin AA, Mochalov DV, Gapontsev VP. Industrial grade 100 kW power CW fiber laser, in Proc Adv Solid-State Lasers Congr Tech Dig, San Diego, CA, USA 2013; paper ATh4A.2.
[19] Hajireza P, Forbrich A, Zemp R. In-Vivo functional optical-resolution photoacoustic microscopy with stimulated Raman scattering fiber-laser source. Biomed Opt Express 2014;5(2):539–46. https://doi.org/10.1364/BOE.5.000539.
[20] Kong C, Pilger C, Hachmeister H, Wei X, Cheung TH, Lai CSW, et al. Compact fs ytterbium fiber laser at 1010 nm for biomedical applications. Biomed Opt Express 2017;8(11):4921–32. https://doi.org/10.1364/BOE.8.004921.
[21] Zervas MN. High power ytterbium-doped fiber lasers - Fundamentals and applications. Int J Mod Phys B 2014;28(12):1442009. https://doi.org/10.1142/S0217979214420090.
[22] Kir'yanov AV, Barmenkov YO, Villegas-Garcia IL, Cruz JL, Andres MV. Highly Efficient Holmium-Doped All-Fiber ~2.07-μm Laser Pumped by Ytterbium-Doped Fiber Laser at ~1.13 μm. IEEE J Select Topics Quant Electron 2018;24(5):0903108. https://doi.org/10.1109/JSTQE.2018.2810385.
[23] Kopyeva MS, Filatova SA, Kamynin VA, Trikshev AI, Kozlikina EI, Astashov VV, et al. Ex Vivo Exposure to Soft Biological Tissues by the 2-μm All-Fiber Ultrafast Holmium Laser System. Appl Science 2022;12(8):3825. https://doi.org/10.3390/app12083825.
[24] Du X, Zhang H, Wang X, Zhou P, Liu Z. Short cavity-length random fiber laser with record power and ultrahigh efficiency. Opt Lett 2016;41(3):571–4. https://doi.org/10.1364/OL.41.000571.
[25] Chen Y, Fan C, Yao T, Xiao H, Leng J, Zhou P, et al. Brightness enhancement in random Raman fiber laser based on a graded-index fiber with high-power multimode pumping. Opt Lett 2021;46(5):1185–8. https://doi.org/10.1364/OL.416740.
[26] Sinha S, Langrock C, Digonnet MJF, Fejer MM, Byer RL. Efficient yellow-light generation by frequency doubling a narrow-linewidth 1150 nm ytterbium fiber oscillator. Opt Lett 2006;31(3):347–439. https://doi.org/10.1364/OL.31.000347.
[27] Bacher C, Oliveira R, Nogueira RN, Romano V, Ryser M. Yellow light generation by frequency doubling of a fiber oscillator. Proc SPIE 2016;9893:989303. https://doi.org/10.1117/12.2230681.
[28] Goodman JW. Statistical Optics. New York: Wiley; 2000.
[29] Pietralunga SM, Martelli P, Martinelli M. Photon statistics of amplified spontaneous emission in a dense wavelength-division multiplexing regime. Opt Lett 2003;28(3):152–4. https://doi.org/10.1364/OL.28.000152.
[30] Valero N, Marion D, Lhermite J, Delagnes JC, Renard W, Royon R, et al. High-power amplified spontaneous emission pulses with tunable coherence for efficient non-linear processes. Sci Rep 2021;11:4844. https://doi.org/10.1038/s41598-021-83443-2.
[31] Kablukov SI, Zlobina EA, Podivilov EV, Babin SA. Output spectrum of Yb-doped fiber lasers. Opt Lett 2012;37(13):2508–10. https://doi.org/10.1364/OL.37.002508.
[32] Barmenkov YO, Muniz-Cánovas P, Kir'yanov AV, Carrascosa AA, Cruz JL, Andrés MV. Coexistence of quasi-CW and SBS-boosted self-Q-switched pulsing in Ytterbium-doped fiber laser with low Q-factor cavity. J Lightw Technol 2020;38(14):3751–8. https://doi.org/10.1109/JLT.2020.2980480.
[33] Solli DR, Ropers C, Koonath P, Jalali B. Optical rogue waves. Nature 2007;450:1054–8. https://doi.org/10.1038/nature06402.
[34] Akhmediev N, Kibler B, Baronio F, Belić M, Zhong WP, Zhang Y, et al. Roadmap on optical rogue waves and extreme events. J Opt 2016;18:063001. https://doi.org/10.1088/2040-8978/18/6/063001.
[35] Tlidi M, Taki M. Rogue waves in nonlinear optics. Adv Opt Photon 2022;14(1):87–147. https://doi.org/10.1364/AOP.438025.
[36] Kelson I, Hardy A. Optimization of Strongly Pumped Fiber Lasers. J Lightw Technol 1999;17(5):891–7. https://doi.org/10.1109/50.762908.
[37] Cimek J, Liaros N, Couris S, Stępień R, Klimczak M, Buczyński R. Experimental investigation of the nonlinear refractive index of various soft glasses dedicated for development of nonlinear photonic crystal fibers. Opt Mater Express 2017;7:3471–83. https://doi.org/10.1364/OME.7.003471.
[38] Agrawal, G. P. *Nonlinear Fiber Optics*. 3rd ed. (San Diego: Academic Press, ch. 4, 2001).
[39] Minguela-Gallardo JA, Barmenkov YO, Kir'yanov AV, Beltrán-Pérez G. Photon statistics of actively Q-switched erbium-doped fiber laser. J Opt Soc Amer B 2017;34(7):1407–14. https://doi.org/10.1364/JOSAB.34.001407.